HHS Public Access

Author manuscript

Nat Chem Biol. Author manuscript; available in PMC 2017 June 19.

Published in final edited form as:

Nat Chem Biol. 2017 February ; 13(2): 150–152. doi:10.1038/nchembio.2262.

A fluorescent probe for cysteine depalmitoylation reveals dynamic APT signaling

Rahul S. Kathayat[1], **Pablo D. Elvira**[1], and **Bryan C. Dickinson**[1,*]

[1]Department of Chemistry, The University of Chicago, Chicago, IL 60637

Abstract

Hundreds of human proteins are modified by reversible palmitoylation of cysteine residues (*S*-palmitoylation), but the regulation of depalmitoylation is poorly understood. Here, we develop "depalmitoylation probes" (DPPs), small molecule fluorophores to monitor the endogenous activity levels of "erasers" of *S*-palmitoylation, acyl-protein thioesterases (APTs). Live-cell analysis with DPPs reveals rapid growth factor-mediated inhibition of the depalmitoylation activity of APTs, exposing a novel regulatory mechanism of dynamic lipid signaling.

Palmitoylation and depalmitoylation of cysteine residues on target proteins plays a key role in regulating protein localization, trafficking, and resultant cell signaling.[1-4] Recent advances in mass spectrometry-based protein profiling techniques have greatly expanded the catalog of human proteins modified by *S*-palmitoylation to include hundreds of putative targets.[5,6] The Asp-His-His-Cys (DHHC)-containing protein acyltransferases (DHHC-PATs) are the "writers" that install the lipid modification, of which there are 23 members in human.[7] Acyl-protein thioesterases (APTs) are the "erasers" of *S*-palmitoylation,[1] including the lyosomal degradation enzyme protein palmitoylthioesterase-1[8] and the putatively cytosolic proteins APT1 and APT2, which are part of the metabolic serine hydrolase (mSH) superfamily.[9] In addition, three previously uncharacterized enzymes were recently identified as regulators of N-Ras depalmitoylation and are potentially additional *S*-palmitoylation erasers.[10]

The APT enzymes have been proposed to contain no substrate specificity and act constitutively to depalmitoylate proteins universally from intracellular membranes.[11] However, several lines of evidence suggests that *S*-palmitoylation is, in fact, regulated and dynamic, including findings that PSD-95 is rapidly depalmitoylated following glutamate stimulation,[12] that activation of FGF receptors by FGF2 leads to palmitoylation of cell adhesion molecules in neurons,[13] and that T-cell activation induces accelerated palmitate

*Corresponding author Dickinson@uchicago.edu (Bryan C. Dickinson).

AUTHOR CONTRIBUTIONS

R.S.K. and P.D.E. synthesized all compounds in the paper. R.S.K. performed all analytical measurements, *in vitro* assays, and cell culture experiments. R.S.K. and B.C.D. designed experimental strategies and wrote the paper.

COMPETING FINANCIAL INTERESTS

The authors declare no competing financial interests.

cycling.[14] Indeed, the APT enzymes themselves can be *S*-palmitoylated,[15] potentially resulting in auto-regulatory mechanisms. To address the roles of APT activities in cell signaling, several classes of small molecule inhibitors have been developed, including the pan-depalmitoylase inhibitor PalmB and the APT1 and APT2 specific inhibitors ML348 and ML349.[16-19]

Current approaches to study S-palmitoylation primarily involve proteomics, monitoring the trafficking of microinjected fluorescent substrates,[17,20] or the use of cell-permeable substrate mimetics.[21] These approaches reveal the balance between palmitoylation and depalmitoylation, but cannot reveal potential upstream regulatory mechanisms specifically of the depalmitoylases. Therefore, to study the regulation and dynamics of *S*-palmitoylation, there is a need for methods to monitor the activity levels of depalmitoylases in physiological contexts. Here, we present the development and application of depalmitoylation probes (DPPs), a new family of molecular imaging reagents that report on endogenous levels of depalmitoylation activity in live cells. We go on to deploy one new probe, DPP-3, to discover that growth factor stimulation results in a rapid decrease of depalmitoylation activity in epidermoid carcinoma (A431) cells, uncovering a new mechanism regulating lipid signaling.

To generate a fluorescent probe for *S*-depalmitoylation activity, we envisioned a live cell-deployable synthetic substrate for the APT enzymes that becomes fluorescent upon depalmitoylation. Fluorescent probes for redox status have been developed which rely on the ability of thiols to cleave carbamates, which are otherwise stable in biological conditions, via a five-membered ring nucleophilic attack.[22] We envisioned a probe design in which a modified cysteine residue is appended to a pro-fluorescent molecule via a carbamate linker, such that enzymatic release of the thiol on the cysteine triggers a rapid cyclization reaction and release of a fluorescent product (Fig. 1a). Based on this concept, we designed and synthesized depalmitoylation probe-1 (DPP-1, **1**), which features a palmitoylated cysteine residue tethered to *N,N*-dimethyl rhodol via a carbamate linker (Fig. 1a, Supplementary Note).

As expected, the carbamate modification on DPP-1 forces the rhodol fluorophore into the lactone form, which has minimal visible absorbance and very low fluorescence (Supplementary Results, Supplementary Fig. 1). However, incubation of 5 μM DPP-1 with either 50 nM APT1 or 50 nM APT2 (Supplementary Fig. 2) resulted in an ~250-fold enhancement in fluorescence signal after 20 min (Fig. 1b, Supplementary Fig. 3). These data validate the general design strategy and confirm DPP-1 is a good substrate for *in vitro* APT biochemical assays, but the poor water solubility of DPP-1, as indicated by the requirement of detergents to run *in vitro* assays, precluded utility in live cell contexts. To improve water solubility, we assayed whether the probe required a palmitoylated cysteine residue for enzyme activity, or whether a shorter lipid chain could suffice. We synthesized depalmitoylation probe-2 (DPP-2, **2**), which has a C7-lipid rather than a C15-lipid (Fig. 1a, Supplementary Note). *In vitro* assays with purified APTs revealed that DPP-2 in fact functions slightly better than DPP-1 as a substrate, possibly due to improved solubility (Fig. 1c, Supplementary Fig. 1).

To improve APT1 target engagement, we synthesized depalmitoylation probe-3 (DPP-3, **3**) (Fig. 1a, Supplementary Note), which features an additional lysine residue based on both the natural N-Ras substrate and pharmacological data.[16] *In vitro* assays of DPP-3 revealed striking reaction kinetics with APT1 (Fig. 1d) and a modest selectivity for APT1 over APT2, confirming target engagement can be tuned by modifications proximal to the acyl cysteine. More critically, both DPP-2 and DPP-3 are water soluble, allowing the enzymatic assays to be performed in the absence of detergents (Supplementary Fig. 4). To confirm the *in vitro* response of the DPPs, catalytically inactivating point mutations (Supplementary Figs. 2 and 5) and inhibitors (Supplementary Fig. 6) abrogate the DPP signal. Given that DPP-2 and DPP-3 show a 200- and 400-fold enhancement in fluorescence (Supplementary Fig. 3), respectively, after 20 min of reaction with 50 nM APT1 and function in water, we next pursued live-cell experiments.

In order to determine whether DPP-2 and DPP-3 could detect endogenous APT activities in live cells, we first used HEK293T cells as a model cell line. Incubation of HEK293T cells with 1 μM DPP-2 for 15 m resulted in robust intracellular fluorescent signal as monitored by live cell fluorescence microscopy (Fig. 2a, Supplementary Figs. 7 and 8) or flow cytometry (Supplementary Fig. 9), confirming the presumed high basal activity of APTs. Critically, the signal is perturbed by inhibition with 2 μM PalmB, 5 μM ML348, or 5 μM ML349. DPP-3 also functions in live cells, except inhibition with lower amounts of PalmB or ML348 were needed to perturb the signal (Fig. 2b and c, Supplementary Figs. 10 and 11), likely due to better uptake of DPP-2 (Supplementary Fig. 12). Moreover, the DPP-3 signal is not substantially perturbed by the APT2 inhibitor ML349 (Fig. 2c), suggesting DPP-3 selectivity in live cells mirrors what was observed *in vitro*. To further validate the inhibitor experiments, we found that RNAi knockdown of APT1 blocks the DPP-3 signal similarly to ML348 (Fig. 2d, Supplementary Fig. 13). However, neither APT1 knockdown or ML348 treatment blocked the signal to the level of PalmB treatment, likely due to either APT2 or other depalmitoylases acting on DPP-3. Finally, to confirm that DPP-3 can function in a variety of cell types, we repeated the flow cytometry experiments in HeLa, MCF-7, and MDA-MB-231 cells, which revealed that DPP-3 can detect endogenous depalmitoylase activities in each of these model cell lines (Supplementary Fig. 14). Collectively, these results confirm that both DPP-2 and DPP-3 can measure endogenous depalmitoylase levels in a variety of cellular contexts.

Encouraged by the performance of DPPs in live cells, we next sought to test the hypothesis that cell signaling events modulate depalmitoylase activity levels. We chose to deploy DPP-3 in epidermoid carcinoma A431 cells, which express high levels of the epidermal growth factor (EGF) receptor, respond to EGF stimulation, and are devoid of endogenous mutations of *HRAS*, *KRAS* and *NRAS*. We hypothesized that DPP-3 is detecting the APT(s) that regulate *NRAS*, since the probe was designed based on this substrate, and that if S-palmitoylation signaling is indeed regulated at the depalmitoylase level, cells with normal Ras signaling would be more likely to show an effect. We serum starved A431 cells to make them susceptible to transient activation by EGF, which intriguingly resulted in an increase in basal depalmitoylase activity levels, which is knocked down by inhibition with PalmB or M348 to similar levels as non-serum starved cells (Fig. 2e,f, Supplementary Fig. 15). Even

more striking, we discovered that stimulation of serum starved cells with 1 ng/mL EGF for 15 min results in an inhibition of depalmitoylation activity (Fig. 2g,h, Supplementary Fig. 16), confirming the hypothesis that APTs are in fact dynamically regulated by upstream signaling events.

The discovery of EGF-induced deactivation of depalmitolyation activity supports a proposed model in which membrane-bound proteins are activated via enhanced membrane retention through inhibition of APTs[23] (Fig. 2i). It is unknown where in the cell the DPP signals are arising from, thus it is unclear what mechanisms are controlling the change or how these results effect downstream signaling. However, the finding that depalmitoylation is dynamically regulated in such a temporally dynamic manner indicates deeper investigation is warranted. The next steps are to uncover the mechanisms that mediate the observed APTs activity control, to investigate whether different pools of APT proteins in the golgi, cytoplasm, and cell membrane respond differentially to signaling events, to assay whether other putative depalmitoylases, such as the ABHD17A/B/C proteins, are also regulated in a similar manner, and to test whether other cell types and stimulants generate similar responses. The observation that the depalmitoylation signal from DPP-3 is not completely blocked by APT1 or APT2 modulation, but is substantially blocked by PalmB, suggests that there may be other depalmitoylases yet to be discovered. Development of subcellular targeted, ratiometric, and multicolored DPPs, as well as probes based on other natural palmitoylated substrates, will aid in these research efforts and are currently ongoing. We anticipate that our new general concept of APT probe design, and these first-generation DPPs, will help uncover novel roles and regulatory mechanisms of dynamic lipid signaling. Finally, the general design strategy utilized to create the DPPs opens up the possibility of easily generating fluorescent turn-on probes for the expanding array of dynamic cysteine PTMs[24,25] (Supplementary Fig. 17).

ONLINE METHODS

General materials and methods

Silica gel P60 (SiliCycle, 40-63 μm, 230-400 mesh) was used for column chromatography. Analytical thin layer chromatography was performed using SiliCycle 60 F254 silica gel (precoated sheets, 0.25 mm thick). All chemicals for synthesis were purchased from Sigma-Aldrich (St. Louis, MO) or Fisher Scientific (Pittsburgh, PA) and used as received. ML348 and ML349 were purchased from Tocris (Bristol, UK). EGF was obtained from Gold Biotechnology (Olivette, MO). Synthesis of *N,N*-dimethylrhodol was adapted from previous reports.[26,27] ^{1}H NMR and ^{13}C NMR spectra were collected in NMR solvents $CDCl_3$/CD_3OD/CD_3CN (Sigma-Aldrich, St. Louis, MO) at 25 °C using a 500 MHz Bruker Avance II+ spectrometer with 5 mm QNP probe at the Department of Chemistry NMR Facility at the University of Chicago. ^{1}H-NMR chemical shifts are reported in parts per million (ppm) relative to the peak of residual proton signals from ($CDCl_3$ 7.26 ppm, CD_3OD 3.31 ppm, $(CD_3)_2SO$ 2.50 ppm or CD_3CN 1.94 ppm). Multiplicities are given as: s (singlet), d (doublet), t (triplet), q (quartet), dd (doublet of doublets), m (multiplet). ^{13}C-NMR chemical shifts are reported in parts per million (ppm) relative to the peak of residual proton signals from ($CDCl_3$ 77.16 ppm, CD_3OD 49.0 ppm, $(CD_3)_2SO$ 39.52 ppm or CD_3CN 1.32 and

118.26 ppm). Analysis of NMR was done in iNMR version 5.5.1. and NMR plots were obtained from Topspin 2.1. High resolution mass was obtained from Agilent 6224 TOF High Resolution Accurate Mass Spectrometer (HRA-MS) using combination of APCI and ESI at the Department of Chemistry Mass Spectrometry Facility at the University of Chicago. Low resolution mass spectral analyses and liquid chromatography analysis were carried out on an Advion Expression-L mass spectrometer (Ithaca, NY) coupled with an Agilent 1220 Infinity LC System (Santa Clara, CA). Synthetic procedures and characterization of all compounds shown in Supplementary Note.

Cloning

All plasmids were constructed by Gibson Assembly from PCR products generated using Q5 Hot Start DNA Polymerase (NEB) or Phusion Polymerase (homemade). Plasmids containing the genes for APT1 and APT2 were a gift from Anil Mukherjee. The genes for APT1 and APT2 were cloned into a pET-30 expression vector with a His-tag for purification. Catalytically inactivating mutations S119A and S122A were installed into the expression vectors for APT1 and APT2, respectively. Sequencing was validated at the University of Chicago Comprehensive Cancer Center DNA Sequencing and Genotyping Facility.

Purification of APT1 and APT2

The plasmids for overexpression of APT1 or APT2, or their catalytically inactive mutant forms, were transformed into *E. coli* Rosetta™ DE3. The cells were cultured in 500 mL LB media with 40 μg/mL of kanamycin in a 1 L flask shaking at 37 °C until $OD_{600} \approx 0.6$ and then 1 mM IPTG was added. Cultures were then grown at 18 °C for an additional 20 h. The cells were harvested by centrifugation and lysed by sonication in 30 mL lysis buffer (50mM NaH_2PO_4, 300 mM NaCl, 10% glycerol, pH 7.5). Cell debri was discarded after centrifugation and the lysis supernatant was incubated with 2 mL TALON® Metal Affinity Resin (for APT1 and APT2) or His60 Ni Superflow Resin (for mutant APT1 and APT2) with gentle shaking on ice for 1 h. The His-tagged proteins were purified under standard immobilized metal affinity chromatography (IMAC) by washing and eluting the resin with wash buffer (50 mM NaH_2PO_4, 300 mM NaCl, 10 mM imidazole 5% glycerol, pH 7.5) and elution buffer (50 mM NaH_2PO_4, 300 mM NaCl, 50-300 mM imidazole, 5% glycerol, pH 7.5). The purified proteins were then desalted on GE Disposable PD-10 Desalting Columns and stored in the protein storage buffer (50 mM Tris-HCl, pH 7.5, 300 mM NaCl, 1 mM DTT, 10% Glycerol) at -80 °C. Each purified APT was validated by 12% SDS-PAGE gel for purity (Supplementary Fig. 2). Purified proteins were stored in individual aliquots in protein storage buffer at -80 °C. A fresh aliquot of protein was thawed for each experiment as we observed a time-dependent decline in activity of APT1 and APT2 once thawed.

In vitro kinetic assays and emission spectra of DPP-1, DPP-2, and DPP-3

50 μL of 7.5 μM DPP1-3 in HEPES (20 mM, pH = 7.4, 150 mM NaCl, 0.1% Triton X-100) were added to a 384-well black flat bottom plate (Corning) and placed in an Infinite M200 Pro (Tecan) plate reader at 37 °C for 5 min to warm. 25 μL of either HEPES buffer alone or HEPES buffer containing 150 nM APT1 or APT2, was added using a multi-channel pipette, resulting in a final concentration of 5 μM DPP1-3 and 50 nM APT1 or APT2. Fluorescence

intensities (λ_{ex} 490/9 nm, λ_{em} 545/20 nm, Gain 70, No. of flashes 25, Integration time 100 μs and Z-position 20000 μm) were measured at 30 s time interval for 20 min. At the end of 20 min kinetic run, emission spectra were obtained (λ_{ex} 485 nm, λ_{em} 510-700 nm, Gain 100, No. of flashes 25, Integration time 100 μs and Z-position 20,000 μm). For the catalytically inactive enzyme experiments, 10-times more APT1(S119A) and APT2(S122A) enzyme were used.

In vitro inhibitor assays of DPP-3

20 μL of 300 nM APT1/APT2 in HEPES (20 mM, pH = 7.4, 150 mM NaCl, 0.1% Triton-X 100) were added to 20 μL of buffer/300 μM PalmB/300 μM ML348 and incubated at 37 °C for 30 min. Similarly, for the no APT control, 20 μL buffer was added to 20 μL of buffer containing 0.3% DMSO. 25 μL of the mixture was added to the 50 μL of 7.5 μM DPP-3 in HEPES buffer for a final concentration of 50 μM PalmB/ML348, 50 nM APT1/2, and 5 μM of DPP-3. After incubation for 20 min at 37 °C, 60 μL of each mixture was transferred to a 384-well black flat bottom plate. Fluorescence intensities (λ_{ex} 490/9 nm, λ_{em} 545/20 nm, Gain 70, No. of flashes 25, Integration time 100 μs and Z-position 20,000 μm) were then measured after 10 min.

UV-Vis

UV-Vis measurements were carried out on a Shimadzu UV-2700 UV-VIS spectrophotometer. Samples for absorption measurements were contained in 1 cm × 1 cm quartz cuvettes with 1 cm light path (Hellma analytics). HEPES (20 mM, pH = 7.4, 150 mM NaCl) containing 1% Triton X-100 was used to make dilute solution of DPP1, DPP2 and DPP3 of 1.0 - 0.1 absorbance at 310 nm. Extinction coefficients were calculated by linear least-squares fitting of plots of A *vs.* concentration. All fits gave R^2 values of ≥ 0.999.

Cell culture and maintenance

HEK293T (ATCC), A431 cells (gift from Yamuna Krishnan), MDA-MB-231 and MCF-7 cells (gift from Cellular Screening Center, University of Chicago) and HeLa cells (ATCC) were maintained in DMEM/High Glucose (10% FBS, 1% P/S, L-Glutamine, Sodium pyruvate, Gibco) with 10% FBS (Gibco/Life Technolgies, Qualified US origin) at 37 °C and 5% CO_2. HEK293T, MDA-MB-231, and MCF-7 cells are listed in the database of commonly misidentified cell lines maintained by ICLAC (http://iclac.org/databases/cross-contaminations/). We obtained fresh cells from ATCC or early passage aliquots from the Cellular Screening Center, University of Chicago, which were frozen down at an early passage (passage 5) in individual aliquots. The cells were then used for less than 25 passages for all experiments. Multiple biological replicates were performed with cells from different passages and freshly thawed aliquots. There was no testing for mycoplasma infection or further authentification because early passage cells were used for all experiments.

Fluorescence imaging of DPP-2 and DPP-3

HEK293T (650,000 cells per dish) cells were plated with 1.5 mL of DMEM (High Glucose, 10% FBS) in a 35 mm glass bottom dish (D35-10-1.5-N; Cellvis) 24 hrs prior to imaging. 30 min before the addition of the DPP probe, the cell culture media was removed and cells were

washed with 1 mL of DPBS. The media was then replaced with 1 mL of DMEM containing 1 μM Hoechst 33342 and either 0.1% DMSO carrier as a control, 1 or 2 μM Palm B, 0.1, 1.0, or 5 μM ML348, and incubated for 30 min at 37 °C and 5% CO_2. The media was removed, the cells were washed with 1 mL of Live Cell Imaging Solution (ThermoFisher), and 1 mL of 1 μM DPP-2 or DPP-3 in Live Cell Imaging Solution was added to each plate. For ML348 0.1, 1.0, or 5 μM was added along with DPP-2 or DPP-3. After incubation for 15 min at 37 °C and 5% CO_2, images were obtained on an inverted epi-fluorescence microscope (Olympus IX83) attached with EMCCD camera (Photometrics Evolve Delta) with 40x oil objective (N/A 1.3) for DPP-2 (excitation filter 500/20, dichroic chroma 89007, emission filter 535/30, exposure time 200 ms, EM gain 25), Hoechst 33342: (excitation filter 402/15, emission filter 455/50, dichroic chroma 89013, exposure time 30 ms, EM gain 25), and brightfield (exposure time 5 ms, EM gain 5), and for DPP-3 (exposure time 500 ms, EM gain 150), Hoechst 33342: (exposure time 30 ms, EM gain 25), and brightfield (exposure time 20 ms, EM gain 5). Analyses were performed in ImageJ (Wayne Rasband, NIH). For data analysis, the average fluorescence intensity per image in each experimental condition was obtained by selecting ROIs in the brightfield image. For display, the data were normalized to the average fluorescence intenstiy of the control conditions. Each experiment was repeated at least three separate times with identical results.

Flow cytometry

Cells were plated on a 10 cm dish with 10 mL of DMEM/High Glucose (10% FBS, 1% P/S, L-Glutamine, Sodium pyruvate) 36-48 hours prior to the day of experiment and maintained at 37 °C, 5% CO_2 so as to obtain 80-90% confluency. Cells were washed with DPBS and trypsinized with 1 mL 0.05% Trypsin. 5 mL of DMEM/High Glucose (10% FBS, L-Glutamine, Sodium pyruvate) was added and cells were spun down at 1200 rpm for 3 min. Media was discarded and cells were resuspended in 5 mL of Live Cell Imaging Solution and again spun down at 1200 rpm for 3 min. The cells pellets obtained were resuspended in 3-5 mL of Live Cell Imaging Solution and divided into 500 μL aliquots. The aliquots were treated with either 0.2% DMSO carrier or 1 μM of PalmB/ML348 or 1 μM/5 μM of ML349 inhibitor. After 30 min of incubation at room temperature, 1 μL of 2.5 mM DPP-3 in DMSO was added to each aliquot for a final concentration of 5 μM, and the solutions were mixed. After 5 min incubation at room temperature, fluorescence signal in FITC channel was measured for 10000 cells (5000 for HeLa experiments) on a LSR-Fortessa 4-15 HTS (BD digital instrument, 488 nm laser with 530/30 nm filter for FITC). For analyzing DPP2 in HEK293T cells, the aliquots were treated with either 0.2% DMSO carrier or 2 μM of PalmB, 5 or 20 μM of ML348/ML349 and then analyzed by the protocol as mentioned above. Data was analyzed by FlowJo software version 10.0.8. For comparison of A431 starved versus non-starved, parallel 10 cm dishes of A431 cells were plated in 10 mL of DMEM (high glucose, 10% FBS, 1% P/S), and grown for 36 h. The growth media was removed, and replaced by 10 mL of either DMEM (High glucose) with 10% FBS to maintain “growth” conditions, or DMEM (High glucose) without FBS respectively for “starvation” conditions, and incubated for 14 h. After trypsinization, both plates were treated with 5 mL of DMEM (high glucose) for spinning the cells down, and further processing and analysis were performed as described above by flow cytometry.

APT1 RNAi by fluorescence microsopy

30,000 cells per well were plated in 250 μL DMEM glutamax (high glucose, 10% FBS) in an 8-well imaging dish (Lab-Tek Chambered Coverglass, Thermo Scientific). After 12 h, the cells were transfected with 5 pmol control/APT1 siRNA using Lipofectamine RNAi Max using the standard protocol. After 48 h the media was replaced by 1 μM Hoechst 33342 in 300 μL DMEM, high glucose. After 15 min of incubation at 37 °C, the cells were washed with 1 mL of Live Cell Imaging Solution and replaced by 5 μM DPP3 in Live Cell Imaging Solution. After 15 min of incubation at room temperature, images were obtained on an inverted epi-fluorescence microscope (Olympus IX83) attached with EMCCD camera (Photometrics Evolve Delta) with 40x oil objective (N/A 1.3) for DPP-3 (excitation filter 500/20, dichroic chroma 89007, emission filter 535/30, exposure time 100 ms, EM gain 50), Hoechst 33342: (excitation filter 402/15, emission filter 455/50, dichroic chroma 89013, exposure time 40 ms, EM gain 30), and brightfield (exposure time 30 ms, EM gain 10). Analyses were performed in ImageJ (Wayne Rasband, NIH). For data analysis, the average fluorescence intensity per image in each experimental condition was obtained by selecting ROIs in the brightfield image, and the data was normalized to the average fluorescence intensity of the control siRNA conditions. The experiment was repeated in three biological replicates.

APT1 RNAi by flow cytometery

350,000 cells per well were plated in 2 mL DMEM glutamax (high glucose, 10% FBS) in a 6-well dish. After 12 h, the cells were transfected with 30 pmol control/APT1 siRNA using Lipofectamine RNAi Max using the standard protocol. After 48 h the media was removed, the cells were washed with 1.5 mL of DPBS, and removed from the plate by incubation with 200 μL of 0.05% trypsin. The cells were resuspended in 1.2 mL DMEM glutamax (high glucose, 10% FBS) and centrifuged at 500 rcf for 3 min. The supernatent was discarded, the cells were washed twice with 1 mL of Live Cell Imaging Solution, and the cell pellet was then resuspended in Live Cell Imaging Solution to generate 500 μL aliquots. 1 μL of 2.5 mM DPP-3 in DMSO was added to each aliquot for a final concentration of 5 μM. After 5 min incubation at room temperature, fluorescence signal in the FITC channel was measured for 10,000 cells on a LSR-Fortessa 4-15 HTS (BD digital instrument, 488 nm laser with 530/30 nm filter for FITC). Data was analyzed by FlowJo software version 10.0.8.

Starvation and EGF stimulation of A431 Cells

Parallel 35 mm glass bottom dishes (D35-10-1.5-N; Cellvis) of A431 cells (450,000) were plated in 2 mL of DMEM glutamax (high glucose, 10% FBS, 1% P/S), and grown for 36 h. The growth media was removed, and replaced by 1.5 mL of either DMEM (High glucose) with 10% FBS to maintain “growth” conditions, or DMEM (High glucose) without FBS respectively for “starvation” conditions, and incubated for 24 h. The media was replaced by 1 mL of “growth” or “starvation” media containing 1 μM Hoechst 33342. After incubation for 15 min at 37 °C, the media from both the serum starved or full serum dishes was removed, and the cells were washed with 1 mL Live cell imaging solution. 1 mL Live Cell Imaging Solution containing 5 μM DPP-3 was then added and the dish was incubated at room termpature for 15 minutes. For EGF stimulation experiments, two parallel dishes of

cells were serum starved, then incubated with DPP-3 in either the absence or the presence of 1 ng/mL EGF. The cells were then imaged for DPP-3 (excitation filter 500/20, dichroic chroma 89007, emission filter 535/30, exposure time 150 ms, EM gain 50), Hoechst 33342: (excitation filter 402/15, emission filter 455/50, dichroic chroma 89013, exposure time 25 ms, EM gain 30), and brightfield (exposure time 20 ms, EM gain 10 for starvation experiment or exposure time 5 ms, EM gain 5 for EGF stimulation experiment). For data analysis, the average fluorescence intensity per image in each experimental condition was obtained by selecting ROIs in the brightfield image. For display, the data were normalized to the average fluorescence intensity of the control conditions. For the starvation experiments, the non-starved cells were used as the control conditions and arbitrarily set to '100', while for the EGF stimulation experiments the starved, no EGF cells were used as the reference control. Each separate experiment was repeated at least three times. The data from each biological replicate for the EGF stimulation was analyzed individually and is shown in Supplementary Fig. 16. The average results from the three biological replicate experiments for both experiments were analyzed in batch and is shown in Fig. 2f, h.

Supplementary Material

Refer to Web version on PubMed Central for supplementary material.

Acknowledgments

This work was supported by the University of Chicago, the National Institute Of General Medical Sciences of the National Institutes of Health (R35 GM119840), the University of Chicago Medicine Comprehensive Cancer Center (P30CA14599), and a "Catalyst Award" from the Chicago Biomedical Consortium, with support from the Searle Funds at The Chicago Community Trust. We thank Jinyue Pu and Darby Dammeier for technical assistance, and Chuan He, Anil Mukherje, Yamuna Krishnan, and Jared Lewis for supplying materials and equipment.

References

1. Linder ME, Deschenes RJ. Palmitoylation: policing protein stability and traffic. Nat Rev Mol Cell Biol. 2007; 8:74–84. [PubMed: 17183362]
2. Eisenberg S, Laude AJ, Beckett AJ, Mageean CJ, Aran V, Hernandez-Valladares M, Henis YI, Prior IA. The role of palmitoylation in regulating Ras localization and function. Biochem Soc Trans. 2013; 41:79–83. [PubMed: 23356262]
3. Topinka JR, Bredt DS. N-terminal palmitoylation of PSD-95 regulates association with cell membranes and interaction with K+ channel Kv1.4. Neuron. 1998; 20:125–134. [PubMed: 9459448]
4. Chan P, Han X, Zheng B, DeRan M, Yu J, Jarugumilli GK, Deng H, Pan D, Luo X, Wu X. Autopalmitoylation of TEAD proteins regulates transcriptional output of the Hippo pathway. Nat Chem Biol. 2016; 12:282–289. [PubMed: 26900866]
5. Peng T, Thinon E, Hang HC. Proteomic analysis of fatty-acylated proteins. Curr Opin Chem Biol. 2016; 30:77–86. [PubMed: 26656971]
6. Hernandez JL, Majmudar JD, Martin BR. Profiling and inhibiting reversible palmitoylation. Curr Opin Chem Biol. 2013; 17:20–26. [PubMed: 23287289]
7. Zheng B, DeRan M, Li X, Liao X, Fukata M, Wu X. 2-Bromopalmitate analogues as activity-based probes to explore palmitoyl acyltransferases. J Am Chem Soc. 2013; 135:7082–7085. [PubMed: 23631516]
8. Verkruyse LA, Hofmann SL. Lysosomal targeting of palmitoyl-protein thioesterase. J Biol Chem. 1996; 271:15831–15836. [PubMed: 8663305]

9. Long JZ, Cravatt BF. The metabolic serine hydrolases and their functions in mammalian physiology and disease. Chem Rev. 2011; 111:6022–6063. [PubMed: 21696217]
10. Lin DT, Conibear E. ABHD17 proteins are novel protein depalmitoylases that regulate N-Ras palmitate turnover and subcellular localization. Elife. 2015; 4:e11306. [PubMed: 26701913]
11. Rocks O, Gerauer M, Vartak N, Koch S, Huang ZP, Pechlivanis M, Kuhlmann J, Brunsveld L, Chandra A, Ellinger B, Waldmann H, Bastiaens PI. The palmitoylation machinery is a spatially organizing system for peripheral membrane proteins. Cell. 2010; 141:458–471. [PubMed: 20416930]
12. El-Husseini Ael D, Schnell E, Dakoji S, Sweeney N, Zhou Q, Prange O, Gauthier-Campbell C, Aguilera-Moreno A, Nicoll RA, Bredt DS. Synaptic strength regulated by palmitate cycling on PSD-95. Cell. 2002; 108:849–863. [PubMed: 11955437]
13. Ponimaskin E, Dityateva G, Ruonala MO, Fukata M, Fukata Y, Kobe F, Wouters FS, Delling M, Bredt DS, Schachner M, Dityatev A. Fibroblast growth factor-regulated palmitoylation of the neural cell adhesion molecule determines neuronal morphogenesis. J Neurosci. 2008; 28:8897–8907. [PubMed: 18768683]
14. Zhang MM, Tsou LK, Charron G, Raghavan AS, Hang HC. Tandem fluorescence imaging of dynamic S-acylation and protein turnover. Proc Natl Acad Sci U S A. 2010; 107:8627–8632. [PubMed: 20421494]
15. Kong E, Peng S, Chandra G, Sarkar C, Zhang Z, Bagh MB, Mukherjee AB. Dynamic palmitoylation links cytosol-membrane shuttling of acyl-protein thioesterase-1 and acyl-protein thioesterase-2 with that of proto-oncogene H-ras product and growth-associated protein-43. J Biol Chem. 2013; 288:9112–9125. [PubMed: 23396970]
16. Davda D, Martin BR. Acyl protein thioesterase inhibitors as probes of dynamic S-palmitoylation. Medchemcomm. 2014; 5:268–276. [PubMed: 25558349]
17. Dekker FJ, Rocks O, Vartak N, Menninger S, Hedberg C, Balamurugan R, Wetzel S, Renner S, Gerauer M, Scholermann B, Rusch M, Kramer JW, Rauh D, Coates GW, Brunsveld L, Bastiaens PI, Waldmann H. Small-molecule inhibition of APT1 affects Ras localization and signaling. Nat Chem Biol. 2010; 6:449–456. [PubMed: 20418879]
18. Rusch M, Zimmermann TJ, Burger M, Dekker FJ, Gormer K, Triola G, Brockmeyer A, Janning P, Bottcher T, Sieber SA, Vetter IR, Hedberg C, Waldmann H. Identification of acyl protein thioesterases 1 and 2 as the cellular targets of the Ras-signaling modulators palmostatin B and M. Angew Chem Int Ed Engl. 2011; 50:9838–9842. [PubMed: 21905186]
19. Adibekian A, Martin BR, Chang JW, Hsu KL, Tsuboi K, Bachovchin DA, Speers AE, Brown SJ, Spicer T, Fernandez-Vega V, Ferguson J, Hodder PS, Rosen H, Cravatt BF. Confirming target engagement for reversible inhibitors in vivo by kinetically tuned activity-based probes. J Am Chem Soc. 2012; 134:10345–10348. [PubMed: 22690931]
20. Gormer K, Burger M, Kruijtzer JA, Vetter I, Vartak N, Brunsveld L, Bastiaens PI, Liskamp RM, Triola G, Waldmann H. Chemical-biological exploration of the limits of the Ras de- and repalmitoylating machinery. Chembiochem. 2012; 13:1017–1023. [PubMed: 22488913]
21. Creaser SP, Peterson BR. Sensitive and rapid analysis of protein palmitoylation with a synthetic cell-permeable mimic of SRC oncoproteins. J Am Chem Soc. 2002; 124:2444–2445. [PubMed: 11890786]
22. Lee JH, Lim CS, Tian YS, Han JH, Cho BR. A two-photon fluorescent probe for thiols in live cells and tissues. J Am Chem Soc. 2010; 132:1216–1217. [PubMed: 20052975]
23. Dekker FJ, Hedberg C. Small molecule inhibition of protein depalmitoylation as a new approach towards downregulation of oncogenic Ras signalling. Bioorg Med Chem. 2011; 19:1376–1380. [PubMed: 21129981]
24. Paulsen CE, Carroll KS. Cysteine-mediated redox signaling: chemistry, biology, and tools for discovery. Chem Rev. 2013; 113:4633–4679. [PubMed: 23514336]
25. Lin H, Su X, He B. Protein lysine acylation and cysteine succination by intermediates of energy metabolism. ACS Chem Biol. 2012; 7:947–960. [PubMed: 22571489]
26. Sauers RR, Husain SN, Piechowski AP, Bird GR. Shaping the absorption and fluorescence bands of a class of efficient, photoactive chromophores: synthesis and properties of some new 3H-xanthen-3. Dyes and Pigments. 1987; 8:35–53.

27. Smith GA, Metcalfe JC, Clarke SD. The design and properties of a series of calcium indicators which shift from rhodamine-like to fluorescein-like fluorescence on binding calcium. Journal of the Chemical Society, Perkin Transactions. 1993; 2:1195–1204.

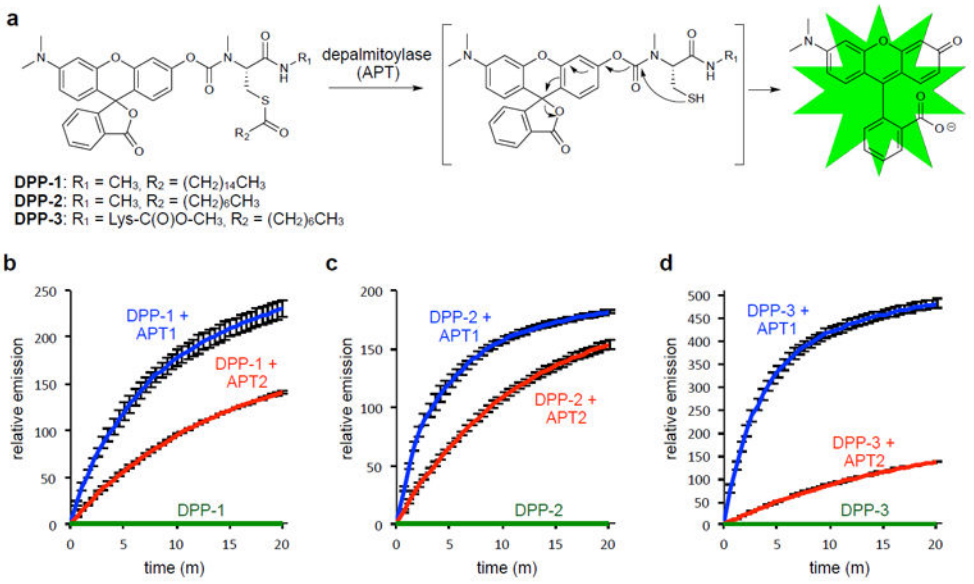

Figure 1.

Design and *in vitro* validation of DPPs. (**a**) Schematic of design and mechanism of fluorescent probes for cysteine deacylase activity. A cysteine residue is tethered to a pro-fluorescent molecule by a biologically stable carbamate linker. Deacylase activity on the cysteine releases the thiol form of the probe, which rapidly cyclizes, breaks the carbamate, and releases a fluorescent product. The physical and biological properties of the molecule can be tuned by modulating the acyl modification on the thiol (R_1) and the C-terminal amide modification on the cysteine (R_2). Structures of DPP-1, DPP-2, and DPP-3, a family of fluorescent probes for cysteine depalmitoylation, are shown. (**b-d**) *In vitro* fluorescence assays of 5 μM DPP-1 (b), DPP-2 (c), or DPP-3 (d) in HEPES (20 mM, pH 7.4, 150 mM NaCl, 0.1% Triton X-100) with either 50 nM purified APT1 or APT2 (λ_{ex} 490/9 nm, λ_{em} 545/20 nm). Error bars are standard deviation (n = 3).

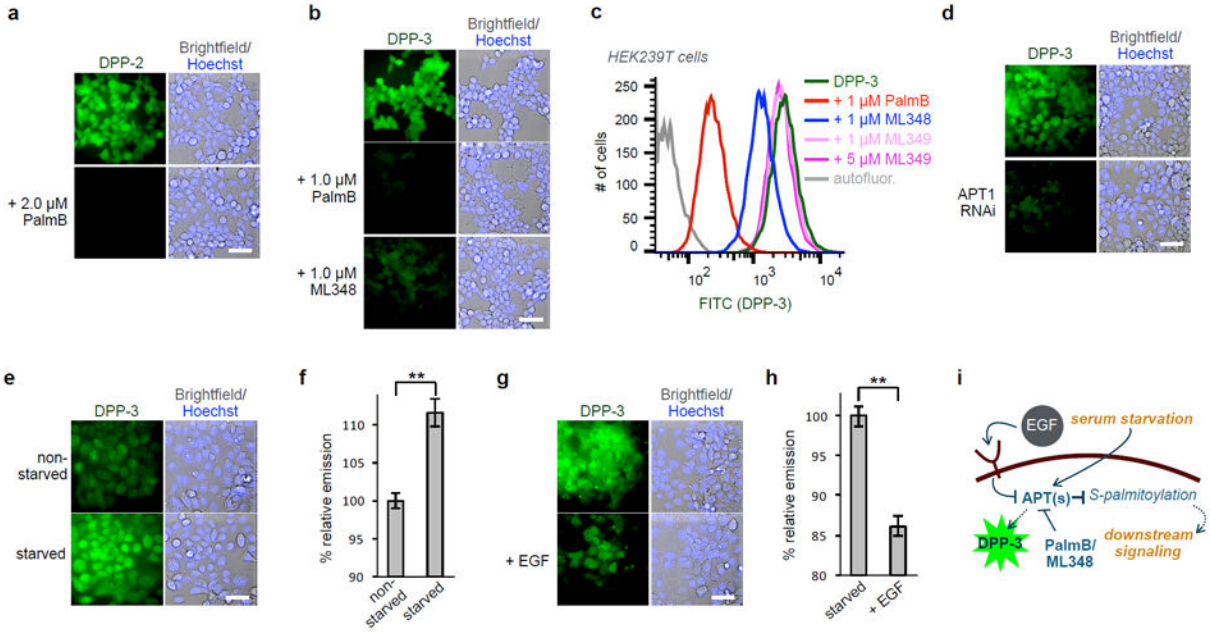

Figure 2.

Analysis of endogenous and growth factor-stimulated depalmitoylase activities using DPPs. (**a**) HEK293T cells loaded with 1 μM DPP-2 for 15 m, after treatment with either DMSO or PalmB, and then analyzed by fluorescence microscopy. (**b**) HEK293T cells loaded with 1 μM DPP-3 for 15 m, after treatment with either DMSO, PalmB, or ML348, and then analyzed by fluorescence microscopy. (**c**) HEK293T cells loaded with 5 μM DPP-3 for 5 min after treatment with either DMSO, PalmB, ML348, or ML349, and then analyzed by flow cytometry. (**d**) HEK293T cells treated with control/APT1 targeting RNAi for 48 h loaded with 5 μM DPP-3 for 15 m and then analyzed by fluorescence microscopy. (**e**) A431 cells grown in normal media conditions or serum starved for 24 h loaded with 5 μM DPP-3 for 15 m and then analyzed by fluorescence microscopy. (**f**) Quantification of experiment shown in (e). (**g**) Serum starved A431 cells loaded with 5 μM DPP-3 for 15 m in either the absence or presence of 1 ng/mL EGF and then analyzed by fluorescence microscopy. (**h**) Quantification of experiment shown in (**g**). (i) Schematic of proposed EGF-induced depalmitoylation signaling through transient deactivation of APTs. Error bars in (f) and (h) are ± std. error (n = 15 data points, three biological replicates), Statistical analyses performed with a two-tailed Student's *t*-test with unequal variance, ** *P* value < 0.0001. 50 μm scale bar shown in images.